Geophysical Prospecting

EAGE EUROPEAN ASSOCIATION OF GEOSCIENTISTS & ENGINEERS

Geophysical Prospecting, 2015 doi: 10.1111/1365-2478.12258

Shallow virtual source redatuming by multi-dimensional deconvolution

Joost van der Neut[1]*, Dmitri Alexandrov[2] and Andrey Bakulin[3]

[1]*Department of Geoscience and Engineering, Delft University of Technology, Stevinweg 1, 2628 CN Delft, The Netherlands,* [2]*Earth's Physics Department, St. Petersburg State University, Ulyanovskaya Street 1, St. Petersburg 198504, Russia, and* [3]*Saudi Aramco, EXPEC Advanced Research Center, Geophysics Technology, Saudi Arabia*

Received February 2014, revision accepted January 2015

ABSTRACT

Recently, new on-shore acquisition designs have been presented with multi-component sensors deployed in the shallow sub-surface (20 m–60 m). Virtual source redatuming has been proposed for these data to compensate for surface statics and to enhance survey repeatability. In this paper, we investigate the feasibility of replacing the correlation-based formalism that undergirds virtual source redatuming with multi-dimensional deconvolution, offering various advantages such as the elimination of free-surface multiples and the potential to improve virtual source repeatability. To allow for data-driven calibration of the sensors and to improve robustness in cases with poor sensor spacing in the shallow sub-surface (resulting in a relatively high wavenumber content), we propose a new workflow for this configuration. We assume a dense source sampling and target signals that arrive at near-vertical propagation angles. First, the data are preconditioned by applying synthetic-aperture-source filters in the common receiver domain. Virtual source redatuming is carried out for the multi-component recordings individually, followed by an intermediate deconvolution step. After this specific pre-processing, we show that the downgoing and upgoing constituents of the wavefields can be separated without knowledge of the medium parameters, the source wavelet, or sensor characteristics. As a final step, free-surface multiples can be eliminated by multi-dimensional deconvolution of the upgoing fields with the downgoing fields.

INTRODUCTION

Bakulin and Calvert (2006) introduced the virtual source method in which sources are redatumed from the Earth's surface to a downhole receiver array. Since the required redatuming operators are actually recorded, this type of redatuming can be implemented without knowledge of the propagation velocity above the receivers. Redatumed signals can be used for migration (Zhou *et al.* 2006) or travel-time tomography (Hanafy and Schuster 2007; Byun, Yu, and Seol 2010; Tatanova, Mehta, and Kashtan 2011). Since the virtual source method is relatively well repeatable, it has also proven useful for reservoir monitoring (Bakulin *et al.* 2007; Mehta *et al.* 2008; Korneev *et al.* 2008). Recently, novel onshore acquisition designs have been presented that utilize downhole receivers in shallow sections of the subsurface (20-60m) in complex karsted desert environments (Berron *et al.* 2012). Virtual source redatuming has been proposed for these data as a means to improve survey repeatability (Bakulin *et al.* 2012). Initial tests on synthetic data have shown that multiple reflections from the free surface can be harsh in this environment (Alexandrov, Bakulin, and Burnstad 2012). Conventional demultiple methods, such as surface-related multiple elimination (SRME) (Verschuur, Berkhout, and Wapenaar 1992; Kelamis and Verschuur 2000) appear unfavourable due to the complexity of the upper sub-surface section.

Traditionally, the virtual source method is applied by cross-correlation (Korneev and Bakulin 2006; Schuster and Zhou 2006). Free-surface multiples should be eliminated prior to redatuming, intrinsic losses are not accounted for, and

*E-mail: j.r.vanderneut@tudelft.nl

significant scattering is required to compensate for one-sided illumination (Wapenaar 2006). If these assumptions are not fulfilled, retrieved gathers can be blurred and can contain spurious events. To deblur the retrieved data and to eliminate spurious events, it can be beneficial to replace cross-correlation by multidimensional deconvolution (Wapenaar *et al.* 2011). To facilitate this process, downgoing and upgoing waves should be separated by wavefield decomposition of the multi-component recordings.

In this paper, we adapt the processing sequence for multi-dimensional deconvolution for configurations with shallow downhole receiver arrays. Since the receivers are buried within the first hundred meters of the subsurface, the incident wavefields inherit a relatively high wavenumber content. Unfortunately, the receiver spacing is relatively sparse for this configuration (with 30-m spacing in the example that follows), resulting in severe spatial aliasing. Since the target signals tend to arrive at the receiver array with incident angles that are close to vertical (up to approximately 15° in the example) (Alexandrov *et al.* 2012) and since sources are densely distributed at the surface (with 7.5-m spacing in the example) (Bakulin *et al.* 2012), we can tackle these problems by preconditioning the data with synthetic-aperture-source filters. Moreover, we apply wavefield decomposition after an intermediate redatuming step in which we deconvolve the source and receiver signatures in a natural way. Unlike existing methodologies, this approach requires no knowledge of the source wavelet, the medium parameters, or the multicomponent sensor characteristics, resulting in a completely data-driven workflow.

We start the paper with four theoretical sections, where the concepts of wavefield decomposition, the virtual source method, multi-dimensional deconvolution, and preconditioning by synthetic-aperture-source filters are briefly introduced. In the methodology section that follows, these concepts are combined to build a new workflow for buried sensor arrays in the shallow subsurface. Finally, we demonstrate this workflow with a synthetic example that is based on a recent experiment over an on-shore oilfield in Saudi Arabia.

WAVEFIELD DECOMPOSITION

Consider a Cartesian coordinate system $\mathbf{x} = (x_1, x_2, x_3)$, where x_1 and x_2 are horizontal coordinates and x_3 is the vertical coordinate. Sources are situated at surface locations $\mathbf{x}_S$. Receivers are situated at $\mathbf{x}$ in a horizontal array in the subsurface. Consider the downhole pressure field $P(\mathbf{x}, \mathbf{x}_S; \omega)$ from source $\mathbf{x}_S$ to receiver $\mathbf{x}$, given in the frequency-space domain, where ω is the angular frequency. The pressure field consists of downgoing (superscript $+$) and upgoing (superscript $-$) constituents, according to

$$P(\mathbf{x}, \mathbf{x}_S; \omega) = P^+(\mathbf{x}, \mathbf{x}_S; \omega) + P^-(\mathbf{x}, \mathbf{x}_S; \omega). \quad (1)$$

The vertical particle-velocity field V_3 (where subscript 3 denotes the vertical direction) is related to the pressure field through the equation of motion:

$$V_3(\mathbf{x}, \mathbf{x}_S; \omega) = \frac{-1}{j\omega\rho(\mathbf{x})}\partial_3 P(\mathbf{x}, \mathbf{x}_S; \omega). \quad (2)$$

Here, j is the imaginary unit, $\rho(\mathbf{x})$ is the density along the receiver array, and ∂_3 is a spatial derivative in the vertical direction at $\mathbf{x}$. We introduce the one-way wave equation (Fishman 1991; Haines and de Hoop 1996; Wapenaar 1998):

$$\partial_3 P^{\pm}(\mathbf{x}, \mathbf{x}_S; \omega) = \mp j\mathcal{H}_1(\mathbf{x}; \omega) P^{\pm}(\mathbf{x}, \mathbf{x}_S; \omega). \quad (3)$$

In this expression, $\mathcal{H}_1(\mathbf{x}; \omega)$ is the square root of the Helmholtz operator, given by

$$\mathcal{H}_1(\mathbf{x}; \omega) = \sqrt{\frac{\omega^2}{c^2(\mathbf{x})} + \rho(\mathbf{x})\partial_1\frac{1}{\rho(\mathbf{x})}\partial_1 + \rho(\mathbf{x})\partial_2\frac{1}{\rho(\mathbf{x})}\partial_2}, \quad (4)$$

where $c(\mathbf{x})$ is the space-dependent velocity, and ∂_1 and ∂_2 are spatial derivatives over horizontal coordinates at $\mathbf{x}$. The square root of the Helmholtz operator can be computed

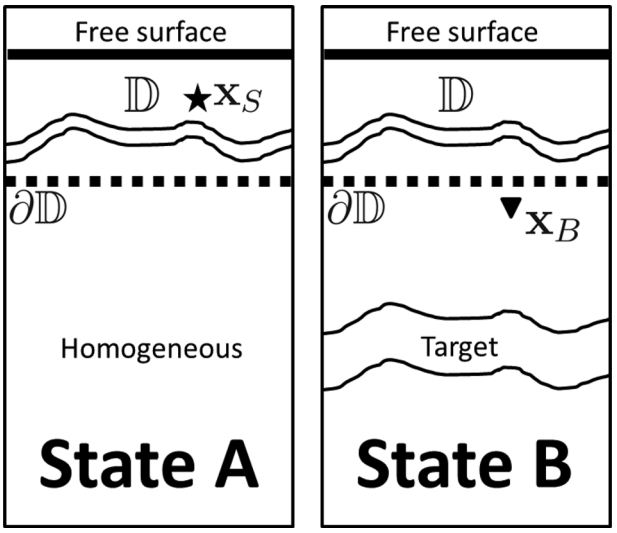

Figure 1 Configuration for the convolution-based representation. Integration volume $\mathbb{D}$ is bound by $\partial\mathbb{D}$ and the free surface. In state A, the medium parameters are identical to those of the physical medium above $\partial\mathbb{D}$ and homogeneous below $\partial\mathbb{D}$. In state B, the medium parameters are identical to those of the physical medium above and below $\partial\mathbb{D}$. The source location $\mathbf{x}_S$ and receiver location $\mathbf{x}_B$ are inside and outside the integration volume, respectively.

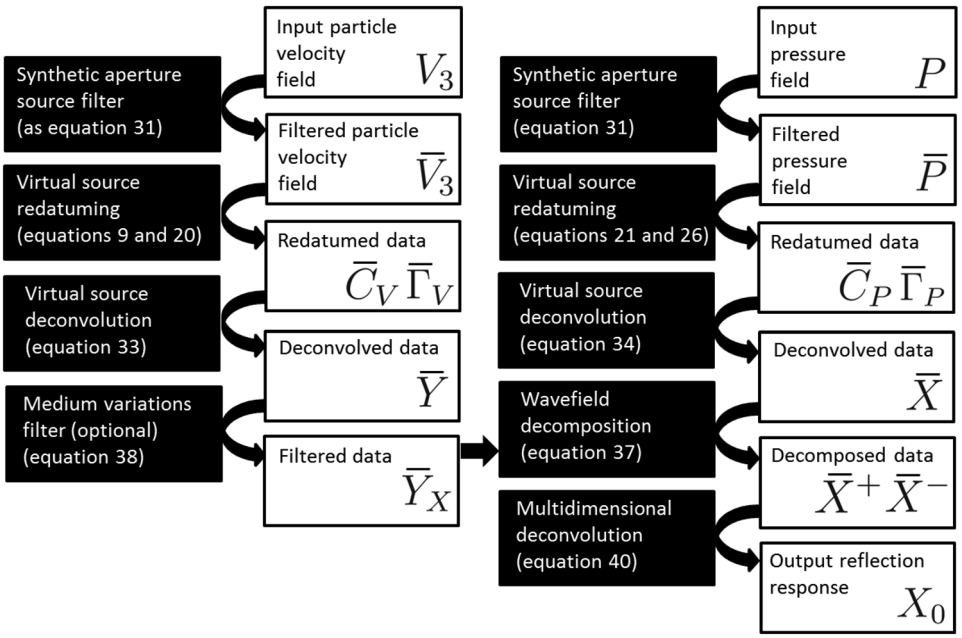

Figure 2 Proposed workflow for data-driven multi-dimensional deconvolution with shallow downhole receiver arrays. Inputs the recorded pressure P and verticle particle velocity V_3. The output is the multiple-free reflection response X_0. References to the relevant equations are given, and a more complete description can be found in the main text.

numerically (Fishman, McCoy, and Wales 1987; Grimbergen, Dessing, and Wapenaar 1998). We filter the particle-velocity field with $\mathcal{H}_1(\mathbf{x};\omega)^{-1}\omega\rho(\mathbf{x})$ and define the result as

$$V_{3P}\left(\mathbf{x},\mathbf{x}_S;\omega\right)=\mathcal{H}_1^{-1}(\mathbf{x};\omega)\omega\rho(\mathbf{x})V_3\left(\mathbf{x},\mathbf{x}_S;\omega\right), \tag{5}$$

where subscript P denotes (pressure-normalized) filtering. In this paper, we define filter $\mathcal{H}_1^{-1}$ for propagating waves only. Additional regularization can be applied to avoid numerical instability due to horizontal wave propagation. By substituting equations (1) and (3) into equation (2) and applying $\mathcal{H}_1(\mathbf{x};\omega)^{-1}\omega\rho(\mathbf{x})$ to the result, it follows that

$$V_{3P}\left(\mathbf{x},\mathbf{x}_S;\omega\right)=P^+\left(\mathbf{x},\mathbf{x}_S;\omega\right)-P^-\left(\mathbf{x},\mathbf{x}_S;\omega\right). \tag{6}$$

Hence, the filtered particle-velocity field can be interpreted as the subtraction of the upgoing pressure field from the downgoing presure field. Alternatively, the recorded pressure field can be interpreted as the addition of these quantities (see equation 1). By combining equations (1) and (6) in two different ways, it follows that

$$P^{\pm}\left(\mathbf{x},\mathbf{x}_S;\omega\right)=\frac{1}{2}P\left(\mathbf{x},\mathbf{x}_S;\omega\right)\pm\frac{1}{2}V_{3P}\left(\mathbf{x},\mathbf{x}_S;\omega\right). \tag{7}$$

Thus, we have shown that filtering the particle-velocity field as in equation (5) and adding the result to the pressure field yield the downgoing pressure field. Alternatively, subtracting these fields yields the upgoing field. This is the essence of wavefield decomposition (Claerbout 1971). In equation (7), pressure normalization has been imposed, such that the decomposed fields $P^{\pm}$ represent downgoing and upgoing pressure fields. Alternatively, decomposition schemes can be derived to obtain downgoing and upgoing flux-normalized fields that obey additional reciprocity properties (Wapenaar and Grimbergen 1996). If we assume that the angle of incidence of each wavefield constituent is close to zero, the horizontal spatial derivatives vanish such that $\mathcal{H}_1(\mathbf{x};\omega)\approx\frac{\omega}{c(\mathbf{x})}$. In this case, equation (5) can be approximated by

$$V_{3P}\left(\mathbf{x},\mathbf{x}_S;\omega\right)\approx\rho(\mathbf{x})c(\mathbf{x})V_3\left(\mathbf{x},\mathbf{x}_S;\omega\right). \tag{8}$$

Decomposition by equations (7) and (8) is referred to as dual-sensor summation since the raw recordings are simply added and subtracted after scaling with the acoustic impedance $\rho(\mathbf{x})c(\mathbf{x})$. For applications of this concept, see Barr (1997) and Mehta *et al.* (2007).

THE VIRTUAL SOURCE METHOD

To apply the virtual source method, the incident wavefield P_{inc} should be isolated with a time gate. In a strongly heterogeneous medium, the incident wavefield can overlap with upgoing reflections, making such a separation not always trivial (Alexandrov *et al.* 2012). In this paper, we define the incident wavefield as the response from the part of the medium above the receiver level (including the source ghost), as if the

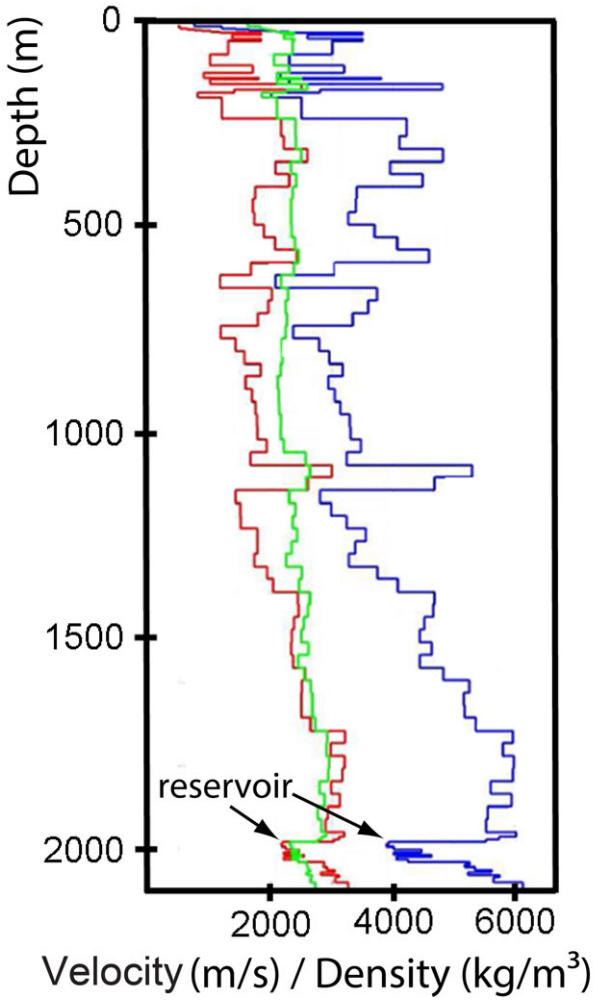

Figure 3 P-wave velocity in m/s (blue), S-wave velocity in m/s (red) and density in kg/m^3 (green) versus depth in m for the layered synthetic model. The location of the reservoir is indicated.

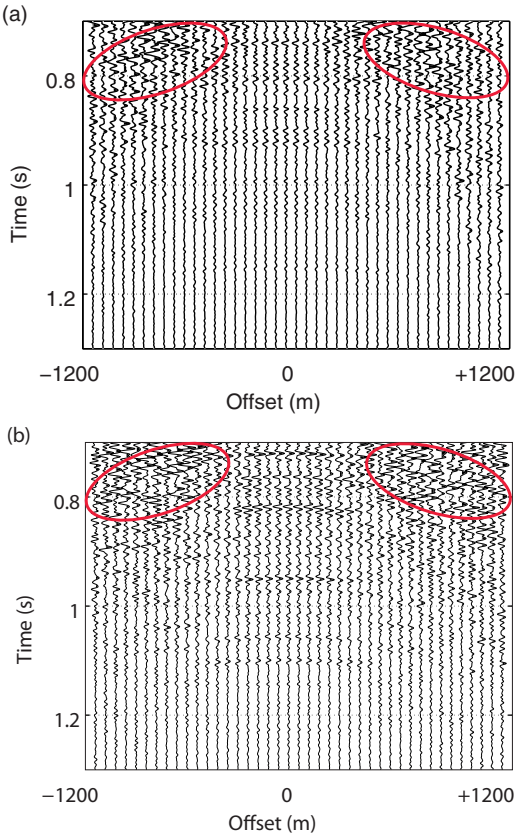

Figure 4 Deep section of a common source gather (with $\mathbf{x}_S$ fixed in the centre of the array). (a) particle velocity $V_3(\mathbf{x}, \mathbf{x}_S; t)$ and (b) pressure $P(\mathbf{x}, \mathbf{x}_S; t)$. The red ellipses indicate events with high propagation angles.

medium below the receiver level were homogeneous. In the virtual source method, the time-gated incident wavefield is cross-correlated with the total field P, followed by a summation over sources. We refer to the result of this operation as the virtual source response C_P (Bakulin and Calvert 2006):

$$C_P(\mathbf{x}_B, \mathbf{x}'_A; \omega) = \sum_s P\left(\mathbf{x}_B, \mathbf{x}_S^{(s)}; \omega\right) P^*_{inc}\left(\mathbf{x}'_A, \mathbf{x}_S^{(s)}; \omega\right), \tag{9}$$

where $\mathbf{x}_B$ and $\mathbf{x}'_A$ are receiver locations, superscript $*$ denotes complex conjugation, subscript P denotes pressure, and s is the source index number. Based on time-reversal logic or a reciprocity theorem of the correlation type (Wapenaar, Fokema, and Snieder 2005; Korneev and Bakulin 2006), $C_P(\mathbf{x}_B, \mathbf{x}'_A; \omega)$ is often interpreted as the response at $\mathbf{x}_B$ to a source at $\mathbf{x}'_A$. In this paper, we interpret the virtual source response differently, based on a reciprocity theorem of the convolution type.

Consider the configuration in Fig. 1. An integration volume $\mathbb{D}$ is enclosed by the free surface and $\partial\mathbb{D}$, being located just above the receiver array. Both boundaries extend to infinity. We introduce the reciprocity theorem of the convolution type (Fokkema and Van den Berg 1993):

$$\begin{aligned}\int_{\mathbb{D}} \{p_A(\mathbf{x};\omega)\, q_B(\mathbf{x};\omega) - q_A(\mathbf{x};\omega)\, p_B(\mathbf{x};\omega)\}\mathrm{d}^3\mathbf{x} \\ = \int_{\partial\mathbb{D}} \{p_A(\mathbf{x};\omega)\, v_{i,B}(\mathbf{x};\omega) - v_{i,A}(\mathbf{x};\omega)\, p_B(\mathbf{x};\omega)\} n_i \mathrm{d}^2\mathbf{x},\end{aligned} \tag{10}$$

where an additional integral over the free surface has been cancelled because of Dirichlet boundary conditions. Here, p_A, $v_{i,A}$, and q_A are the pressure field, the particle-velocity field, and the source distribution in terms of volume injection rate density, respectively, in state A. Subscript B refers to the same

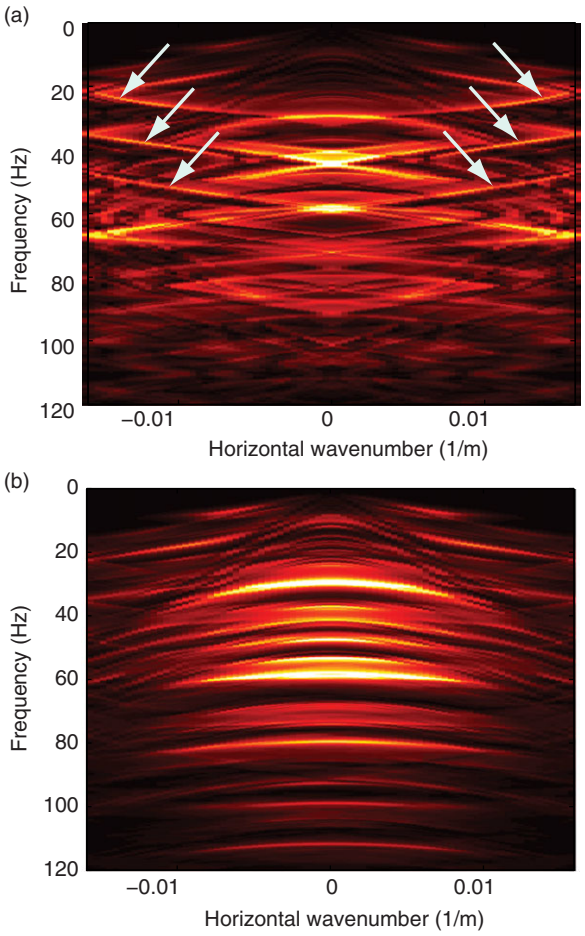

Figure 5 Frequency–wavenumber spectrum of the particle velocity recordings V_3 of a common source gather (with $\mathbf{x}_S$ fixed in the center of the array) (a) before and (b) after synthetic-aperture-source filtering in the common receiver domain with equation (32). The white arrows indicate spatial aliasing. Both gathers are normalized by their maximum amplitude.

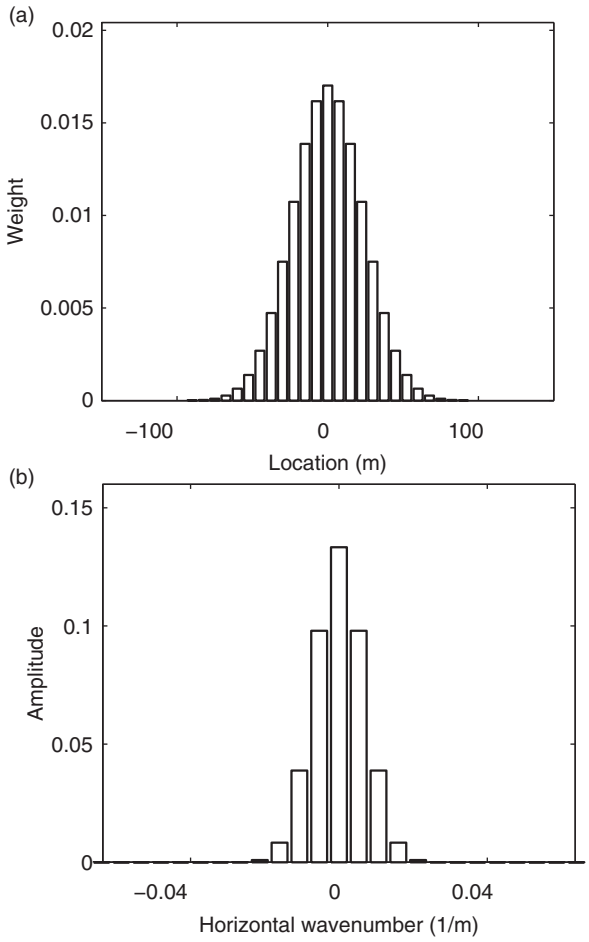

Figure 6 Synthetic-aperture-source filter $B(b)$ in (a) the space domain and (b) the horizontal wavenumber domain. This filter is applied in the common receiver domain with equation (31).

quantities in state B. For the integration path along the receivers, we find $n_i = \delta_{i3}$, being a Kronecker delta function. In state A, we define, pressure field $p_A(\mathbf{x};\omega) = G_{inc}(\mathbf{x}, \mathbf{x}_S;\omega)$, particle-velocity field $v_{i,A}(\mathbf{x};\omega)\, n_i = \frac{-1}{j\omega\rho(\mathbf{x})}\partial_3 G_{inc}(\mathbf{x}, \mathbf{x}_S;\omega)$, and source term $q_A(\mathbf{x};\omega) = \delta(\mathbf{x} - \mathbf{x}_S)$, where $\mathbf{x}_S$ is located inside the volume. Here, G_{inc} is a Green's function of a reference medium that is identical to the physical medium above $\partial\mathbb{D}$ (including the free surface) and homogeneous below $\partial\mathbb{D}$. We assume that this Green's function is related to the time-gated incident field by $P_{inc} = SG_{inc}$, where S is the source wavelet (hence the subscript *inc*, indicating the incident field). In state B, we define, pressure field $p_B(\mathbf{x};\omega) = G(\mathbf{x}, \mathbf{x}_B;\omega)$, particle-velocity field $v_{i,B}(\mathbf{x};\omega)\, n_i = \frac{-1}{j\omega\rho(\mathbf{x})}\partial_3 G(\mathbf{x}, \mathbf{x}_B;\omega)$, and source term $q_B(\mathbf{x}_B;\omega) = \delta(\mathbf{x} - \mathbf{x}_B)$, where $\mathbf{x}_B$ is located outside the integration volume. Here, G is a Green's function of the physical medium. Substitution of these quantities into equation (10) yields

$$G(\mathbf{x}_S, \mathbf{x}_B;\omega) = \int_{\partial\mathbb{D}} \frac{1}{j\omega\rho(\mathbf{x})}[G_{inc}(\mathbf{x}, \mathbf{x}_S;\omega)\{\partial_3 G(\mathbf{x}, \mathbf{x}_B;\omega)\} - \{\partial_3 G_{inc}(\mathbf{x}, \mathbf{x}_S;\omega)\} G(\mathbf{x}, \mathbf{x}_B;\omega)]\mathrm{d}^2\mathbf{x}. \quad (11)$$

We separate the downgoing and upgoing fields at $\mathbf{x}$ (i.e., $G = G^+ + G^-$) and substitute the one-way wave equations $\partial_3 G^{\pm}(\mathbf{x}, \mathbf{x}_B;\omega) = \mp j\mathcal{H}_1(\mathbf{x};\omega) G^{\pm}(\mathbf{x}, \mathbf{x}_B;\omega)$ and $\partial_3 G_{inc}(\mathbf{x}, \mathbf{x}_S;\omega) = -j\mathcal{H}_1(\mathbf{x};\omega) G_{inc}(\mathbf{x}, \mathbf{x}_S;\omega)$, leading to

$$\begin{aligned} G(\mathbf{x}_S, \mathbf{x}_B;\omega) \;= \int_{\partial\mathbb{D}} \frac{1}{j\omega\rho(\mathbf{x})}[&G_{inc}(\mathbf{x}, \mathbf{x}_S;\omega) \\ &\times [j\mathcal{H}_1(\mathbf{x};\omega)\{-G^+(\mathbf{x}, \mathbf{x}_B;\omega) + G^-(\mathbf{x}, \mathbf{x}_B;\omega)\}] \\ &+ [j\mathcal{H}_1(\mathbf{x};\omega) G_{inc}(\mathbf{x}, \mathbf{x}_S;\omega)]\{G^+(\mathbf{x}, \mathbf{x}_B;\omega) \\ &+ G^-(\mathbf{x}, \mathbf{x}_B;\omega)\}]\mathrm{d}^2\mathbf{x}. \end{aligned} \quad (12)$$

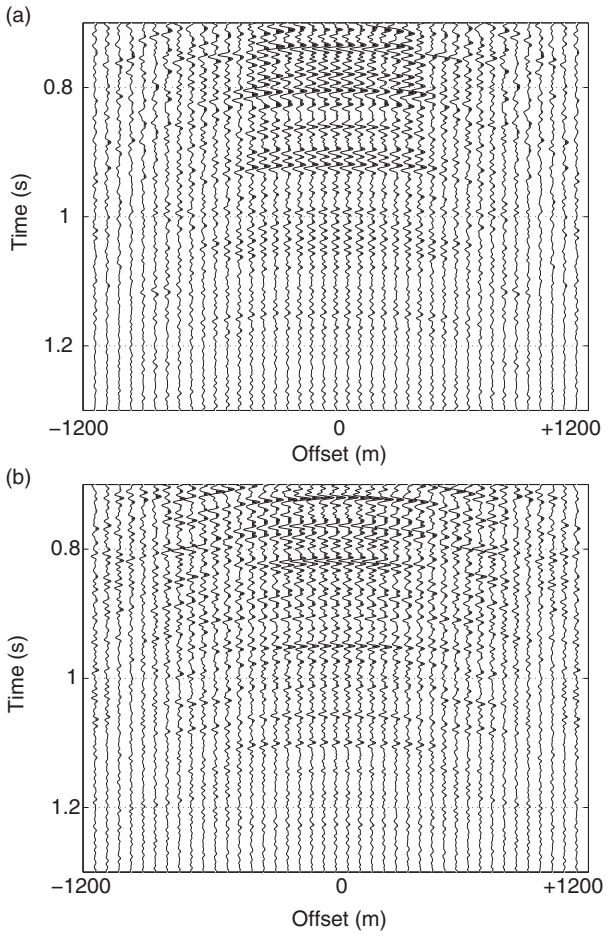

Figure 7 Deep section of a common source gather (with $\mathbf{x}_S$ fixed in the centre of the array) after filtering in the common receiver domain with equation (31). (a) Particle velocity $\bar{V}_3(\mathbf{x}, \mathbf{x}_S; t)$ and (b) pressure $\bar{P}(\mathbf{x}, \mathbf{x}_S; t)$.

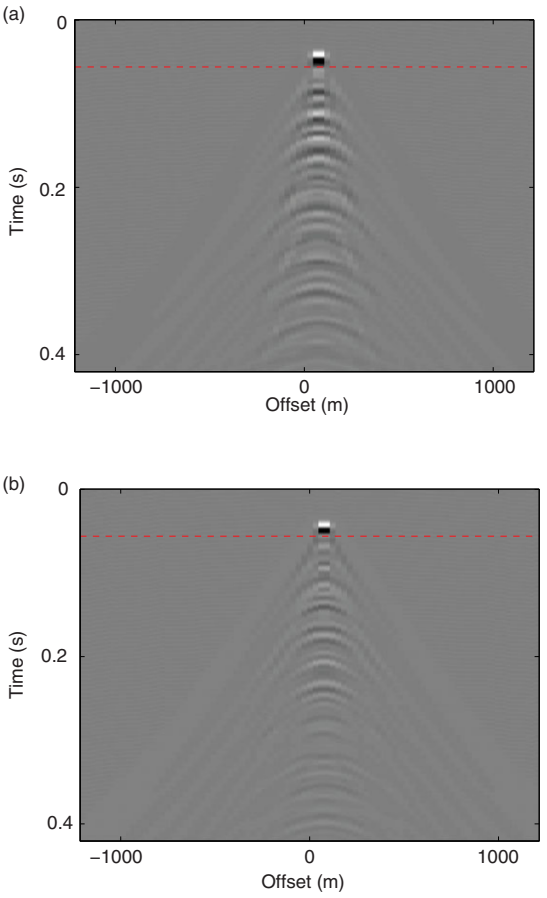

Figure 8 Shallow section of a common source gather (with $\mathbf{x}_S$ fixed in the center of the array) after filtering in the common receiver domain with equation (31): (a) Particle velocity $\bar{V}_3(\mathbf{x}, \mathbf{x}_S; t)$ and (b) pressure $\bar{P}(\mathbf{x}, \mathbf{x}_S; t)$. The time gate is indicated by the red dashed line.

An important property of operator $\mathcal{H}_1$ is its symmetry, in the sense that $\int_{\partial\mathbb{D}} f\,[\mathcal{H}_1 g]\,\mathrm{d}^2\mathbf{x} = \int_{\partial\mathbb{D}} [\mathcal{H}_1 f]\,g\mathrm{d}^2\mathbf{x}$ for any f and g (Wapenaar *et al.* 2011). As a consequence, the convolutions of downgoing fields with downgoing fields in equation 12 cancel and the remaining terms can be merged. We can write the result in two ways:

$$G(\mathbf{x}_B, \mathbf{x}_S; \omega) = \int_{\partial\mathbb{D}} \frac{2}{\omega\rho(\mathbf{x}_A)} [\mathcal{H}_1(\mathbf{x}_A; \omega) G^-(\mathbf{x}_A, \mathbf{x}_B; \omega)] \, G_{inc}(\mathbf{x}_A, \mathbf{x}_S; \omega)\,\mathrm{d}^2\mathbf{x}_A \tag{13}$$

or

$$G(\mathbf{x}_B, \mathbf{x}_S; \omega) = \int_{\partial\mathbb{D}} \frac{2}{\omega\rho(\mathbf{x}_A)} G^-(\mathbf{x}_A, \mathbf{x}_B; \omega)\,[\mathcal{H}_1(\mathbf{x}_A; \omega) \times G_{inc}(\mathbf{x}_A, \mathbf{x}_S; \omega)]\,\mathrm{d}^2\mathbf{x}_A, \tag{14}$$

where we substituted $\mathbf{x}_A = \mathbf{x}$ for notational convenience. We can separate the wavefield at $\mathbf{x}_B$ into downgoing and upgoing constituents, according to

$$G^-(\mathbf{x}_A, \mathbf{x}_B; \omega) = G^{-,+}(\mathbf{x}_A, \mathbf{x}_B; \omega) + G^{-,-}(\mathbf{x}_A, \mathbf{x}_B; \omega). \tag{15}$$

In this representation, $G^{\pm,\pm}$ is the downgoing or upgoing constituent (first superscript) of a Green's function with a downward or upward radiating (second superscript) source. Further, we introduce source–receiver reciprocity, according to

$$G^{-,\pm}(\mathbf{x}_A, \mathbf{x}_B; \omega) = G^{\mp,+}(\mathbf{x}_B, \mathbf{x}_A; \omega). \tag{16}$$

By substitution of equations (15) and (16) into equation (13) and multiplication with the source wavelet S, it follows that

$$P(\mathbf{x}_B, \mathbf{x}_S; \omega) = \int_{\partial\mathbb{D}} X(\mathbf{x}_B, \mathbf{x}_A; \omega)\, P_{inc}(\mathbf{x}_A, \mathbf{x}_S; \omega)\,\mathrm{d}^2\mathbf{x}_A, \tag{17}$$

where $P = SG$ is the pressure field, $P_{inc} = SG_{inc}$ is the incident pressure field that can be isolated by time gating, and

$$X(\mathbf{x}_B, \mathbf{x}_A; \omega) = \frac{2}{\omega\rho(\mathbf{x}_A)}\mathcal{H}_1(\mathbf{x}_A; \omega)\{G^{+,+}(\mathbf{x}_B, \mathbf{x}_A; \omega) + G^{-,+}(\mathbf{x}_B, \mathbf{x}_A; \omega)\}. \quad (18)$$

Equation 17 can be inverted for X by least-squares inversion. With this operation, we remove the incident pressure field from the recorded pressure data. To show this, we derive a normal equation by multiplying both sides of equation (17) with $P^*_{inc}(\mathbf{x}'_A, \mathbf{x}_S; \omega)$ and by summing over sources, yielding

$$C_P(\mathbf{x}_B, \mathbf{x}'_A; \omega) = \int_{\partial\mathbb{D}} X(\mathbf{x}_B, \mathbf{x}_A; \omega)\,\Gamma_P(\mathbf{x}_A, \mathbf{x}'_A; \omega)\mathrm{d}^2\mathbf{x}_A, \quad (19)$$

where C_P is the correlation function as in equation (9) and Γ_P is defined as the point-spread function for pressure fields:

$$\Gamma_P(\mathbf{x}_A, \mathbf{x}'_A; \omega) = \sum_s P_{inc}\left(\mathbf{x}_A, \mathbf{x}_S^{(s)}; \omega\right) P^*_{inc}\left(\mathbf{x}'_A, \mathbf{x}_S^{(s)}; \omega\right). \quad (20)$$

As aforementioned, $C_P(\mathbf{x}_B, \mathbf{x}'_A; \omega)$ is often interpreted as the reflection response at $\mathbf{x}_B$ to a virtual source at $\mathbf{x}'_A$ (Bakulin and Calvert 2006). As we can see from equation (19), C_P is indeed related to reflection response X, but this response is blurred in time and space with the point-spread function. Hence, the point-spread function Γ_P can be interpreted as the radiation pattern of the constructed virtual source. Virtual source focusing can be improved when the correlated data are deconvolved with the point-spread function (Van der Neut 2013). Similar concepts have also been applied to more conventional seismic data, where sources and receivers are both located at the surface. For instance, Henley (2012) demonstrated that deconvolving these data with so-called surface functions can align reflections in complex environments where conventional static corrections tend to fail.

Alternatively, the virtual source method can be applied to the particle velocity records V_3 (where $V_{3,inc}$ is the time-gated incident field). Analogous to equation (9), we define the virtual source response of the vertical particle-velocity fields as

$$C_V(\mathbf{x}_B, \mathbf{x}'_A; \omega) = \sum_s V_3\left(\mathbf{x}_B, \mathbf{x}_S^{(s)}; \omega\right) V^*_{3,inc}\left(\mathbf{x}'_A, \mathbf{x}_S^{(s)}; \omega\right), \quad (21)$$

where subscript V denotes particle velocity. As we did for the pressure fields, the retrieved field C_V can be explained with a convolution-based representation. This is done by substituting equations (15) and (16) into equation (14) and multiplying with the source wavelet S. After substituting $P = SG$ and $P_{inc} = SG_{inc}$, we arrive at

$$P(\mathbf{x}_B, \mathbf{x}_S; \omega) = 2\int_{\partial\mathbb{D}} \{G^{+,+}(\mathbf{x}_B, \mathbf{x}_A; \omega) + G^{-,+}(\mathbf{x}_B, \mathbf{x}_A; \omega)\} \times V_{3,inc}(\mathbf{x}_A, \mathbf{x}_S; \omega)\,\mathrm{d}^2\mathbf{x}_A, \quad (22)$$

where $V_{3,inc}(\mathbf{x}_A, \mathbf{x}_S; \omega) = \frac{1}{\omega\rho(\mathbf{x}_A)}\mathcal{H}_1(\mathbf{x}_A; \omega)P_{inc}(\mathbf{x}_A, \mathbf{x}_S; \omega)$ is the incident particle-velocity field that can be isolated from the data with a time gate. Finally, we apply $\frac{-1}{j\omega\rho(\mathbf{x}_B)}\partial_3^B$ to equation (22) (where superscript B indicates that the partial

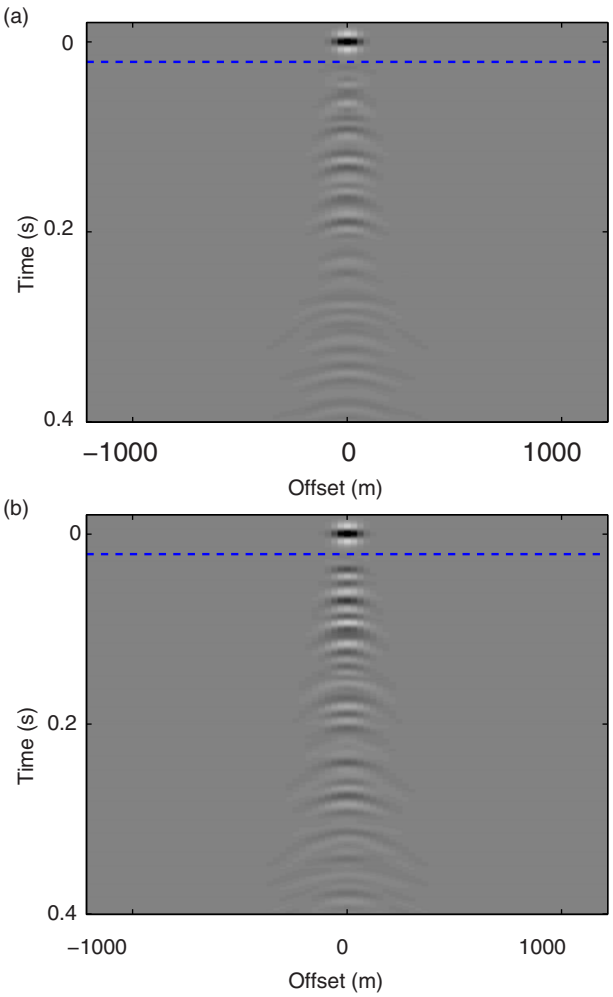

Figure 9 Shallow section of a redatumed common virtual source gather (with $\mathbf{x}_A$ fixed in the centre of the array): (a) $\bar{Y}(\mathbf{x}, \mathbf{x}_A; t)$ and (b) $\bar{X}(\mathbf{x}, \mathbf{x}_A; t)$. Redatuming is applied by equations (9), (20), (21), and (26), followed by 1D deconvolution of equations (33) and (34). Above the dashed blue line we find the source functions of the retrieved fields. We have convolved the gathers with a zero-phase wavelet for visual purposes.

derivative is evaluated at $\mathbf{x}_B$), and we substitute equation (2) (with $\mathbf{x} = \mathbf{x}_B$). This eventually leads to

$$V_3(\mathbf{x}_B, \mathbf{x}_S; \omega) = \int_{\partial\mathbb{D}} Y(\mathbf{x}_B, \mathbf{x}_A; \omega)\, V_{3,inc}(\mathbf{x}_A, \mathbf{x}_S; \omega)\, \mathrm{d}^2\mathbf{x}_A, \quad (23)$$

with

$$Y(\mathbf{x}_B, \mathbf{x}_A; \omega) = \frac{2}{\omega\rho(\mathbf{x}_B)}\mathcal{H}_1(\mathbf{x}_B; \omega)\{G^{+,+}(\mathbf{x}_B, \mathbf{x}_A; \omega) - G^{-,+}(\mathbf{x}_B, \mathbf{x}_A; \omega)\}, \quad (24)$$

where $\partial_3^B G^{\pm,+}(\mathbf{x}_B, \mathbf{x}_A; \omega) = \mp j\mathcal{H}_1(\mathbf{x}_B; \omega)G^{\pm,+}(\mathbf{x}_B, \mathbf{x}_A; \omega)$ (the one-way wave equation) has been substituted. We derive the normal equation of this problem by multiplying equation (23) by $V^*_{3,inc}(\mathbf{x}'_A, \mathbf{x}^{(s)}_S; \omega)$ and summing over the sources, yielding

$$C_V(\mathbf{x}_B, \mathbf{x}'_A; \omega) = \int_{\partial\mathbb{D}} Y(\mathbf{x}_B, \mathbf{x}_A; \omega)\, \Gamma_V(\mathbf{x}_A, \mathbf{x}'_A; \omega)\mathrm{d}^2\mathbf{x}_A, \quad (25)$$

with the point-spread function for particle-velocity fields:

$$\Gamma_V(\mathbf{x}_A, \mathbf{x}'_A; \omega) = \sum_s V_{3,inc}\left(\mathbf{x}_A, \mathbf{x}^{(s)}_S; \omega\right) V^*_{3,inc}\left(\mathbf{x}'_A, \mathbf{x}^{(s)}_S; \omega\right). \quad (26)$$

It can be concluded that, when the virtual source method is applied with pressure fields, we find the sum of the downgoing and upgoing field at $\mathbf{x}_B$ from a downward radiating source at $\mathbf{x}_A$, filtered with $\frac{2}{\omega\rho(\mathbf{x}_A)}\mathcal{H}_1(\mathbf{x}_A; \omega)$ and Γ_P (equations (18) and (19)). Alternatively, when the virtual source method is applied to particle-velocity fields, we find the difference of the downgoing and upgoing fields, filtered with $\frac{2}{\omega\rho(\mathbf{x}_B)}\mathcal{H}_1(\mathbf{x}_B; \omega)$ and Γ_V (equations (24) and (25)). Note that both X and Y could be retrieved from (equations (19) and (25) by inversion.

MULTIDIMENSIONAL DECONVOLUTION

Although the virtual source method has proven to be very effective to remove statics and to improve source repeatability (Bakulin *et al.* 2007), interactions with the free surface are not addressed. Using multi-dimensional deconvolution, we are able to address these interactions during the redatuming process (Wapenaar *et al.* 2011). In this case, we solve the following forward problem

$$P^-(\mathbf{x}_B, \mathbf{x}_S; \omega) = \int_{\partial\mathbb{D}} X_0(\mathbf{x}_B, \mathbf{x}; \omega)\, P^+(\mathbf{x}, \mathbf{x}_S; \omega)\, \mathrm{d}^2\mathbf{x}, \quad (27)$$

with

$$X_0(\mathbf{x}_B, \mathbf{x}; \omega) = \frac{2}{j\omega\rho(\mathbf{x})}\partial_3 G_0(\mathbf{x}_B, \mathbf{x}; \omega). \quad (28)$$

In equation (27), $\partial\mathbb{D}$ is the receiver array, and $\mathbf{x}_B$ is located just below this array (in practice, we generally evaluate $\mathbf{x}_B$ at $\partial\mathbb{D}$). Source locations $\mathbf{x}_S$ are situated at the surface above $\partial\mathbb{D}$. Furthermore, $G_0(\mathbf{x}_B, \mathbf{x}; \omega)$ represents the Green's function with a source at $\mathbf{x}$ and a receiver at $\mathbf{x}_B$ in a reference medium (subscript 0) that is identical to the physical medium below the receiver level and homogeneous above this level. The unknown field X_0 can be retrieved by least-squares inversion of equation (27) for example, see Wapenaar *et al.* (2011) for examples. This approach allows us to eliminate all interactions with the free surface and overburden since X_0 is the response to a medium that is homogeneous above the receiver array.

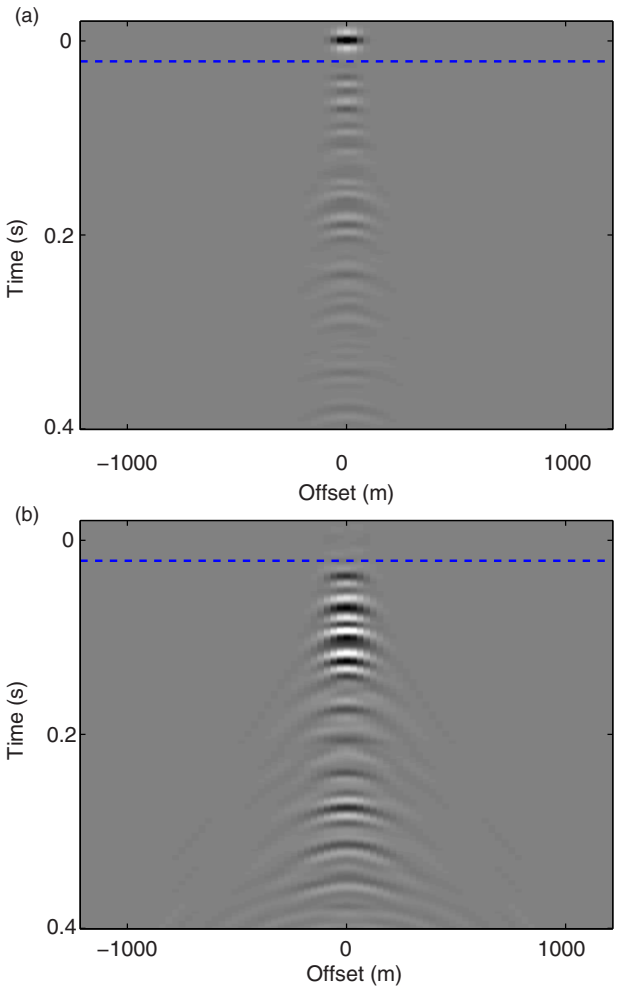

Figure 10 Shallow section of a decomposed common virtual source gather (with $\mathbf{x}_A$ fixed in the center of the array). (a) $\bar{X}^+(\mathbf{x}, \mathbf{x}_A; t)$ and (b) $\bar{X}^-(\mathbf{x}, \mathbf{x}_A; t)$. Decomposition is applied by equation (37) with $\bar{Y} = \bar{Y}_X$. Above the dashed blue line is the source functions of the retrieved fields. Note that the upgoing field contains no source function, as expected. We have convolved the gathers with a zero-phase wavelet for visual purposes.

PRECONDITIONING

To allow inversion, the receiver spacing should be dense enough to avoid spatial aliasing. Therefore, the following Nyquist criterion should be met:

$$\frac{\omega}{c_a} < \frac{\pi}{\Delta x}. \tag{29}$$

Here, Δx is the receiver spacing, and $c_a = c/\sin\alpha_{max}$ is the minimum apparent velocity, with α_{max} being the maximum propagation angle in the data. In modern acquisition designs, as presented by Berron *et al.* (2012), Δx is insufficiently small to satisfy equation (29). As a consequence, the data are spatially aliased, and straightforward inversion is not possible if no additional preconditioning is carried out. We implement such preconditioning by introducing synthetic-aperture sources, being inspired by a similar idea that was recently introduced for an analogous problem in controlled source electromagnetic exploration (Fan *et al.* 2010; Hunziker *et al.* 2012). We make use of the fact that the source array is not spatially aliased. Synthetic-aperture-source data are generated by applying a blurring filter to the forward problem. The blurring filter is constructed by defining the following Gaussian weighting function:

$$B(b) = \frac{1}{\sqrt{2\pi\gamma^2}} \exp\left(\frac{-b^2}{\gamma^2}\right), \tag{30}$$

where parameter γ controls the width of the synthetic-aperture sources and b is an integer. Filter $B(b)$ is applied to the data in the following way:

$$\bar{P}^{\pm}\left(\mathbf{x}, \mathbf{x}_S^{(s)}; \omega\right) = \sum_b P^{\pm}\left(\mathbf{x}, \mathbf{x}_S^{(s-b)}; \omega\right) B(b), \tag{31}$$

where the bar indicates blurred data and s is the source index number. We apply the blurring filter to both sides of equation (27), yielding the preconditioned forward problem:

$$\bar{P}^{-}(\mathbf{x}_B, \mathbf{x}_S; \omega) = \int_{\partial\mathbb{D}} X_0(\mathbf{x}_B, \mathbf{x}; \omega)\, \bar{P}^{+}(\mathbf{x}, \mathbf{x}_S; \omega)\, \mathrm{d}^2\mathbf{x}. \tag{32}$$

Essentially, the filter $B(b)$ suppresses the high-wavenumber content by blending sources. This reduces the maximum propagation angle α_{max} in the data, such that equation (29) is satisfied. As we will show later, X_0 can be retrieved from equation (32) with relatively poor receiver spacing, which is not possible with equation (27) due to spatial aliasing. Velocity filtering is another option that could be applied to remove high wavenumber content prior to inversion. However, velocity filtering often results in additional artefacts, which are naturally avoided by the smooth synthetic-aperture-source filter.

METHODOLOGY

The most straightforward way to retrieve X_0 is to apply wavefield decomposition with equation 7, followed by inversion of equation (27). Although this strategy appeared to be relatively successful when the receiver array is deep and relatively well sampled (Wapenaar *et al.* 2011), the situation is slightly different in cases with coarsely spaced shallow receivers. Moreover, variations in sensor characteristics, coupling, and 3D effects tend to obstruct our workflow. It is particularly hard to preserve the incident wavefield, which is extremely important for the success of multi-dimensional deconvolution (Van der Neut *et al.* 2012). For these reasons, we prefer to develop an alternative workflow by combining different concepts that were discussed in the previous section.

Geophone and hydrophone recordings have different frequency characteristics and therefore should be calibrated. In ocean-bottom cable (OBC) technology, adaptive decomposition schemes are often applied (Schalkwijk, Wapenaar, and Verschuur 2003; Muijs, Robertsson, and Holliger 2004). For borehole data, it is common to apply data matching prior to decomposition (Mehta *et al.* 2010). In practice, however, it appears favorable to apply wavefield decomposition after an intermediate redatuming step. This can be understood intuitively since variations in statics and sensor coupling are removed during redatuming, forcing the signals to align, as they should for a successful wavefield decomposition.

Our workflow utilizes wavefields X and Y, rather than the recorded data P and V_3. This has two advantages. First, each sensor type is deconvolved independently prior to wavefield decomposition. Second, decomposition can be applied without additional knowledge of the medium properties, making the workflow fully data driven. Our scheme assumes wave propagation of the target signals to be close to normal incidence. This assumption is believed to be well fulfilled for this type of data (Alexandrov *et al.* 2012). Medium variations along the receiver array are neglected. If these variations are significant and known, an additional filter is proposed.

Ideally, we would like to retrieve X and Y by inversion of equations (17) and (23). However, since the receiver spacing is relatively poor and the reflecting signals propagate close to vertical for this configuration (with incident angles up until 15° only), we prefer to ignore all off-diagonal elements of the point-spread function (being those entries where $\mathbf{x}'_A \neq \mathbf{x}_A$). This can be done since the point-spread function of the incident wavefield tends to be diagonally dominant. By assuming that $\Gamma_P(\mathbf{x}_A, \mathbf{x}'_A; \omega) = 0$ for any $\mathbf{x}'_A \neq \mathbf{x}_A$, equations (19) and (25) can be approximated by (Van der Neut 2013)

$$C_P(\mathbf{x}_B, \mathbf{x}_A; \omega) \approx X(\mathbf{x}_B, \mathbf{x}_A; \omega)\, \Gamma_P(\mathbf{x}_A, \mathbf{x}_A; \omega), \tag{33}$$

and

$$C_V(\mathbf{x}_B, \mathbf{x}_A; \omega) \approx Y(\mathbf{x}_B, \mathbf{x}_A; \omega)\, \Gamma_V(\mathbf{x}_A, \mathbf{x}_A; \omega), \tag{34}$$

which can be solved by 1D deconvolution. For more details on this approximation (that has also been referred to as diagonal deconvolution) and its relation to other deconvolution-based applications of seismic interferometry, see Van der Neut (2013). This approach appears to be less sensitive to noise than inversion. Spatial aliasing effects are avoided, which is particularly beneficial for the data that we consider in this paper, being sparsely sampled at the receiver side.

We apply $\rho^{-1}(\mathbf{x}_A)\mathcal{H}_1(\mathbf{x}_A;\omega)\mathcal{H}_1^{-1}(\mathbf{x}_B;\omega)\rho(\mathbf{x}_B)$ to $Y(\mathbf{x}_B, \mathbf{x}_A;\omega)$ and refer to this result as

$$Y_X(\mathbf{x}_B, \mathbf{x}_A; \omega) = \rho^{-1}(\mathbf{x}_A)\mathcal{H}_1(\mathbf{x}_A;\omega)\mathcal{H}_1^{-1}(\mathbf{x}_B;\omega)\rho(\mathbf{x}_B) \times Y(\mathbf{x}_B, \mathbf{x}_A; \omega). \tag{35}$$

By substitution of equation (24) into equation (35) it follows that

$$Y_X(\mathbf{x}_B, \mathbf{x}_A; \omega) = \frac{2}{\omega\rho(\mathbf{x}_A)}\mathcal{H}_1(\mathbf{x}_A;\omega)\{G^{+,+}(\mathbf{x}_B, \mathbf{x}_A; \omega) - G^{-,+}(\mathbf{x}_B, \mathbf{x}_A; \omega)\}. \tag{36}$$

By combining equations (18) and (36) in two different ways, we find

$$X^{\pm}(\mathbf{x}_B, \mathbf{x}_A; \omega) = \frac{1}{2}X(\mathbf{x}_B, \mathbf{x}_A; \omega) \pm \frac{1}{2}Y_X(\mathbf{x}_B, \mathbf{x}_A; \omega), \tag{37}$$

where X^+ and X^- are the downgoing and upgoing constituents, respectively, of X. Hence, it follows that the downgoing field X^+ can be obtained by adding X and Y_X. Alternatively, the upgoing field X^- can be obtained by subtracting these fields. To allow for such a decomposition, a filter should be constructed to obtain Y_X from Y. This can be done by numerical computation of the square-root operators in equation (35) (Fishman *et al.* 1987; Grimbergen *et al.* 1998). Alternatively, we can assume that fields propagate close to normal incidence, such that the approximations $\mathcal{H}_1(\mathbf{x}_A;\omega) \approx \frac{\omega}{c(\mathbf{x}_A)}$ and $\mathcal{H}_1(\mathbf{x}_B;\omega) \approx \frac{\omega}{c(\mathbf{x}_B)}$ can be applied. Inserting these approximations into equation (35) yields

$$Y_X(\mathbf{x}_B, \mathbf{x}_A; \omega) \approx \frac{\rho(\mathbf{x}_B)c(\mathbf{x}_B)}{\rho(\mathbf{x}_A)c(\mathbf{x}_A)}Y(\mathbf{x}_B, \mathbf{x}_A; \omega). \tag{38}$$

If the medium parameter variations can be neglected at the receiver level, we find from equation (35) that $Y_X \approx Y$. This approximation has the advantage that no additional information on the propagation velocity and density along the receiver array is required to decompose the wavefields.

Now that we can retrieve the quantities X^- and X^+, we aim to extract the desired reflection response X_0 by multi-dimensional deconvolution. To do this, we revise forward problem (27). This is done by decomposition of equation (17) at $\mathbf{x}_B$ into downgoing and upgoing constituents and substituting the result into equation (27), yielding

$$\int_{\partial\mathbb{D}} X^-(\mathbf{x}_B, \mathbf{x}_A; \omega)\, P_{inc}(\mathbf{x}_A, \mathbf{x}_S; \omega)\, \mathrm{d}^2\mathbf{x}_A = \int_{\partial\mathbb{D}} X_0(\mathbf{x}_B, \mathbf{x}; \omega)\left[\int_{\partial\mathbb{D}} X^+(\mathbf{x}, \mathbf{x}_A; \omega)\, P_{inc}(\mathbf{x}_A, \mathbf{x}_S; \omega)\, \mathrm{d}^2\mathbf{x}_A\right]\mathrm{d}^2\mathbf{x}. \tag{39}$$

We can deconvolve the incident fields at both sides of this equation, bringing us at

$$X^-(\mathbf{x}_B, \mathbf{x}_A; \omega) = \int_{\partial\mathbb{D}} X_0(\mathbf{x}_B, \mathbf{x}; \omega)\, X^+(\mathbf{x}, \mathbf{x}_A; \omega)\, \mathrm{d}^2\mathbf{x}. \tag{40}$$

Theoretically, this equation can be inverted for X_0. Based on this insight, a new workflow for multi-dimensional deconvolution of data from shallow downhole receivers can be derived.

Our workflow is illustrated in Fig. 2. First, the recorded pressure and particle velocity fields are preconditioned by applying a synthetic-aperture-source filter, as in equation (31), to eliminate constituents of the wavefields at high propagation angles. We emphasize that the filter acts on the common receiver gathers, which are assumed to be sampled densely. Next, we isolate the incident fields with a time gate and compute $\bar{C}_P$, $\bar{\Gamma}_P$, $\bar{C}_V$, and $\bar{\Gamma}_V$ with equations (9), (20), (21), and (26) (where bars are added to the field quantities because of the synthetic-aperture-source filter). We refer to this step as virtual source redatuming. Now that the fields are redatumed, we apply single-trace deconvolution of equations (33) and (34), yielding the estimates of $\bar{X}$ and $\bar{Y}$ that we require for wavefield decomposition (once more, with the imprint of the synthetic-aperture-source filter). We can filter $\bar{Y}$ as in equation (38), if an estimate of the impedance contrasts along the receiver array is available. We can also neglect these variations, such that $\bar{Y}_X \approx \bar{Y}$, making the processing scheme fully data driven. Wavefield decomposition can now proceed by adding and subtracting $\bar{X}$ and $\bar{Y}_X$ without further calibration, as in equation (37). Finally, multi- deconvolution can be applied to the decomposed fields $\bar{X}^-$ and $\bar{X}^+$ by multi-trace inversion of equation (40). This yields the desired reflection response X_0. Note that the imprint of the synthetic-aperture-source filter is effectively removed by the inversion (in a similar way as in equation (32)). The advantage of this methodology is that the source signature is not required, the incident wavefield has not

been touched by any decomposition operator, and the sensor characteristics are aligned in a natural way by deconvolution without knowledge of the subsurface parameters at the receiver level. In this sense, we deviate from existing workflows (Wapenaar *et al.* 2011), where wavefield decomposition is applied before redatuming, requiring knowledge of the medium parameters and fine receiver sampling.

EXAMPLE

The following numerical example is based on a recent experiment over an on-shore oilfield in Saudi Arabia that is described in more detail by Alexandrov *et al.* (2012). At the surface, 641 sources are situated with 7.5-m spacing. In an array that is located 30 m below the surface, 81 receivers are deployed with 30-m spacing. The target reservoir is located much deeper in the sub-surface, at 2000m (see Fig. 3). The medium is laterally homogeneous but is characterized by strong vertical contrasts. Because of these contrasts, the downhole responses contain a multitude of horizontally propagating waves, as indicated by the red ellipses in the raw common source gathers of particle velocity and pressure in Fig. 4. Since many constituents of the wavefield have low apparent velocities and the receiver spacing is relatively large, the common source gathers are spatially aliased, which can be seen in the frequency–wavenumber domain, as indicated by the white arrows in Fig. 5(a). However, due to the finer source spacing (7.5 m versus 30 m), the common receiver gathers are not spatially aliased. We design a synthetic-aperture-source filter based on equation (30). In Figure 6(a) we show the filter in the space domain. This filter is applied to the common receiver gathers as demonstrated by equation (31), essentially describing a spatial convolution process. Spatial convolution corresponds to multiplication in the wavenumber domain with the spatial Fourier transform coefficients of the filter that are shown in Fig. 6(b). Note that the filter indeed suppresses high wavenumbers, particularly above the Nyquist wavenumber that follows from the receiver spacing ($1/(2*30m) \approx \pm 0.0167m^{-1}$). Assuming that the reflection response that we aim to retrieve does not contain constituents that are spatially aliased, multi-dimensional deconvolution will remove the imprint of the filter from the data later in the processing sequence, as we will show. The data after synthetic-aperture-source filtering are shown in Fig. 7. Note that the high wavenumber noise (indicated by the red elipses in Fig. 4) has been suppressed. In Figure 5(b) we show the frequency–wavenumber spectrum of the particle-velocity field after filtering. Note that, indeed, the aliased constituents (indicated by the white arrows in Fig. 5a) have been eliminated.

In Figure 8, we zoom in on a shallow section of a common source gather, after filtering in the common receiver domain. We time-gate the incident pressure and particle-velocity fields, as indicated by the dashed red lines in this figure. Virtual source redatuming is applied by equations (9), (20), (21), and (26), followed by 1D deconvolution of equations (33) and (34). Shallow sections of the retrieved fields $\bar{Y}$ and $\bar{X}$ are shown in Fig. 9, containing the retrieved source function around $t = 0s$. Because the medium parameters are constant along the receiver array, it follows that $\bar{Y}_X = \bar{Y}$. Therefore, the fields $\bar{X}$ and $\bar{Y}$ can simply be added and subtracted to retrieve the down- and upgoing wavefields, as described by equation 37. The result of this operation is shown in Fig. 10. Note that the downgoing field contains the source function and multiples from the free surface, whereas the upgoing field contains only reflections (primaries and multiples), as expected. Note that we have not utilized any knowledge of the medium parameters or source signature to achieve this.

Finally, multi-dimensional deconvolution is applied to retrieve the desired multiple-free data X_0. This is done by multi-trace inversion of equation (40). In Fig. 11(a) we show a common virtual source gather as retrieved with the conventional virtual source method (Alexandrov *et al.* 2012). Although the target reflector, indicated by the red arrow, can be identified, multiple reflections pollute the gather. This can be seen when comparing this result with a reference response that was modeled by placing an active source at the virtual source location in a reference medium that is identical to the physical medium below $\partial\mathbb{D}$ and homogeneous above $\partial\mathbb{D}$ (see Fig. 11b). In Fig. 12(a), we show the retrieved upgoing field $\bar{X}^-$. Note that the target reflector can be identified at its correct kinematic position (comparable to Fig. 11a) since the incident field has been removed from the propagation history by virtual source redatuming. We observe various multiple reflections, which can be eliminated by multi-dimensional deconvolution with the downgoing field, yielding X_0 (see Fig. 12b). The spatial imprint of the synthetic-aperture-source filter that is imposed on the gather in Fig. 12(a) is also removed by this operation. Finally, note the good agreement of various events in Fig. 12(b) with those in Fig. 11(b). Horizontally propagating modes have not been retrieved by multi-dimensional deconvolution since they have been eliminated by the synthetic-aperture-source filter.

DISCUSSION

Receiver undersampling is one of the main challenges in applying multi-dimensional deconvolution to data recorded by shallow downhole receiver arrays. Ideally, we would like to

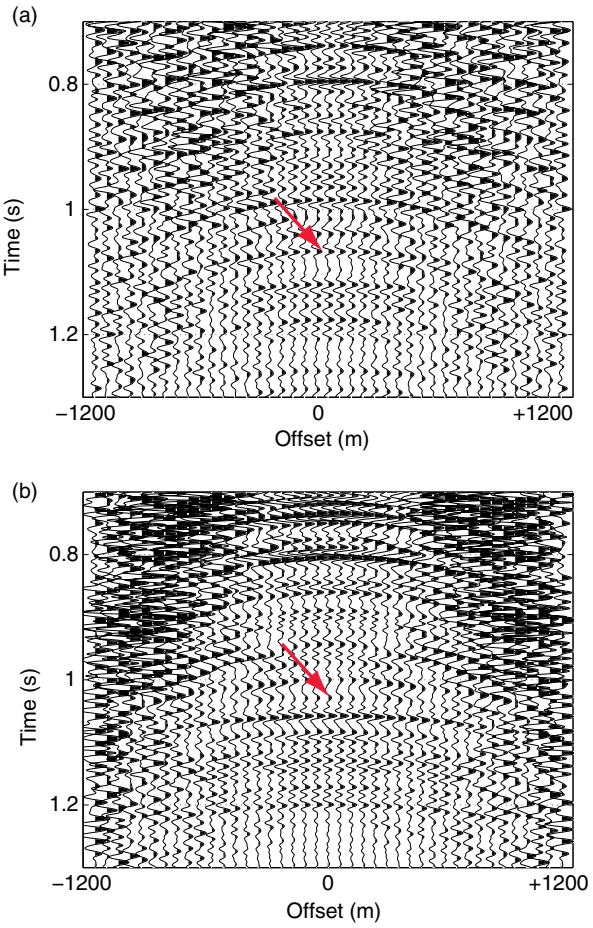

Figure 11 (a) Deep section of a retrieved common virtual source gather (with $\mathbf{x}_A$ fixed in the center of the array) $C_P(\mathbf{x}, \mathbf{x}_A; t)$ by the virtual source method (Alexandrov *et al.* 2012). (b) Reference shot record $X_0(\mathbf{x}, \mathbf{x}_A; t)$ obtained by direct modeling in a medium that is identical to the physical medium but homogeneous above the receiver level. The red arrow indicates the target reflector. We have convolved the gather in panel (b) with a zero-phase wavelet for visual purposes.

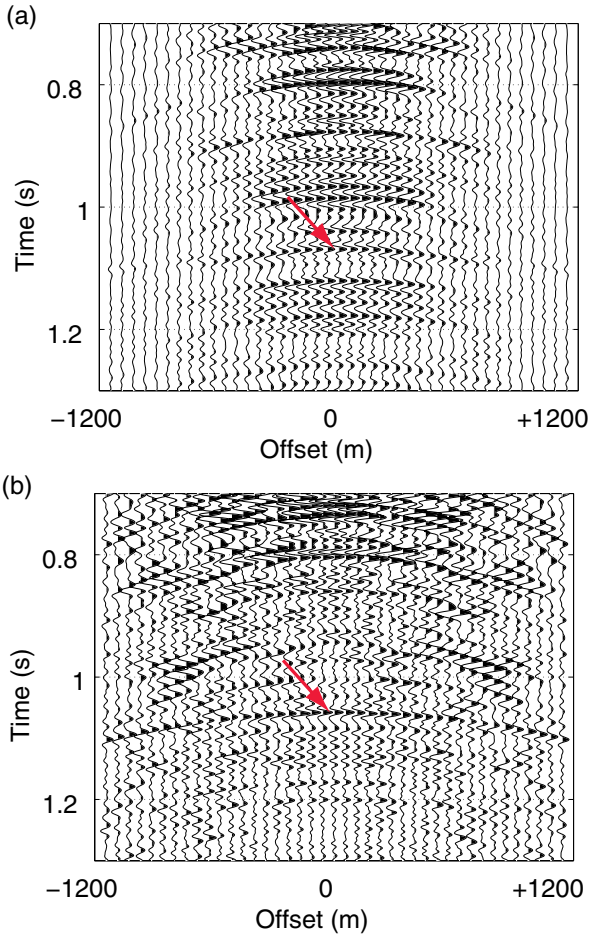

Figure 12 Deep section of a retrieved common virtual source gather (with $\mathbf{x}_A$ fixed in the center of the array). (a) $\bar{X}^{-}(\mathbf{x}, \mathbf{x}_A; t)$ and (b) $X_0^{-}(\mathbf{x}, \mathbf{x}_A; t)$ (obtained by multi-trace inversion of equation 40). The red arrow indicates the target reflector. We have convolved the gathers with a zero-phase wavelet for visual purposes.

satisfy the sampling criterion that was presented in equation (29), but economical reasons often prevent us from doing so. We overcame receiver undersampling with synthetic-aperture-source filters, but this solution is not ideal. We relied heavily on the fact that propagation angles are close to vertical (Alexandrov *et al.* 2012) and that the source array is well sampled. In case of dipping interfaces and lateral heterogeneity, propagation angles at the source and receiver sides can be rather different, and filtering at the source side (as we did) cannot solve the full problem at the receiver side. Another concern is posed by 3D effects. Although implementations in 2D might be a good compromise in some cases, lateral heterogenetiy in the unsampled dimension is not taken into account and can break the validity of the forward problem that we aim to invert. These problems may be overcome by improving the acquisition design with finer receiver spacing and by deploying downhole measurements on a 2D grid. It might also be worthwhile to investigate the feasability of reconstructing wavefields in between the receivers by utilizing the horizontal receiver components, using methodologies that have recently been presented for towed-streamer data (Robertsson *et al.* 2008). Theoretically, multi-dimensional deconvolution can be extended to 3D, although this might be computationally expensive. To meet affordable computational costs, processing could be applied in the plane-wave domain under a layered-medium assumption. Wang *et al.* (2010) have demonstrated that such an approach is computationally feasible in 3D for up/down deconvolution of OBC data.

Isolating the incident wavefield may also not be straightforward. If the shallow subsurface is notoriously complex, the incident wavefield as defined in this paper could contain multiple reverberations that may not be separated from upgoing reflections. For a more thorough discussion on the practice of time-gating in strongly heterogeneous media, see Alexandrov *et al.* (2012). Upgoing constituents of the wavefields may leak into the time-gated gathers, and downgoing constituents that belong to the incident fields may be accidentally excluded. In the proposed methodology, we assume that the time-gated fields inherit the sensor characteristics, such that these could be deconvolved from the field measurements. In case of poor gating, it is questionable how valid this assumption will be. To improve the quality of time-gating, it is recommended to place the receivers in a part of the medium that is relatively homogeneous.

To allow wavefield decomposition without the requirement of additional information on the medium parameters, we have neglected the variations of these parameters along the receiver array. This approach might be reasonable at near offsets, but at far offsets, a different strategy is probably preferred. If estimates of the medium parameters can be provided, these could be incorporated within the proposed scheme, as we suggested. Adding measurements at multiple depth levels or at the surface is another option to constrain the wavefield decomposition problem. Van der Neut *et al.* (2013) presented a data-driven workflow that utilizes measurements at multiple depth levels, and Grobbe *et al.* (2013) extended this workflow for elastodynamic wave propagation. If an estimate can be made of the propagation velocity between the free surface and the receiver level, the free-surface boundary conditions can also be included as an additional constraint for wavefield decomposition. The latter has proven to be an effective strategy for decomposition of towed-streamer data, particularly at low frequencies (Day *et al.* 2013).

With multi-dimensional deconvolution, we aim to remove free-surface multiples from the data by inversion. This method is closely related to the multiple elimination method of Amundsen (2001) that has previously been applied to eliminate multiples from OBC data (Amundsen *et al.* 2001) and towed-streamer data (Majdanski *et al.* 2011). From the marine case, it is well known that the underlying inverse problem is rather ill-posed and that additional constraints in terms of sparsity promotion are very useful (Van Groenestijn and Verschuur 2009; Lin and Herrmann 2013). On a similar note, sparsity promotion can also bring benefits for inverting the type of problem that we discuss in this paper (Van der Neut and Herrmann 2013).

Alternatively, free-surface multiples can be eliminated by prediction and subtraction, as is done in SRME (Verschuur *et al.* 1992). Theoretically, the application of SRME requires knowledge of the source wavelet, which is generally estimated by imposing a minimum-energy criterion on the output gathers. Multiple elimination by inversion does not require information on the wavelet but assumes that the full wavefield (including the incident field) is recorded (Amundsen 2001). In equation (40), we have deghosted the forward problem at the source and receiver sides, and we have removed the source wavelet. Rather than inverting this relation, it could be solved by prediction and subtraction of the free-surface multiples. Unlike in conventional SRME, knowledge of the source wavelet is not required in this case since the source wavelet has already been removed by incident-field deconvolution. To illustrate this, we write the downgoing field as $X^+ = X^+_{inc} + X^+_{sc}$, where X^+_{inc} is the incident downgoing field, and X^+_{sc} is the scattered downgoing field (being the full field minus the incident field). By inspection of equation (17) (where $P = P_{inc} + P_{sc}$ and decomposition can be applied at $\mathbf{x}_B$), it follows that $X^+_{inc}(\mathbf{x}, \mathbf{x}_A; \omega)$ should be a band-limited delta function $\delta(\mathbf{x} - \mathbf{x}_A)$ along the horizontal coordinates $\mathbf{x}$ and $\mathbf{x}_A$. Substituting these quantities into equation (40) yields

$$X^-(\mathbf{x}_B, \mathbf{x}_A; \omega) = \int_{\partial\mathbb{D}} X_0(\mathbf{x}_B, \mathbf{x}; \omega)\,(\delta(\mathbf{x} - \mathbf{x}_A) + X^+_{sc}(\mathbf{x}, \mathbf{x}_A; \omega))\mathrm{d}^2\mathbf{x}. \quad (41)$$

Equation (41) is a Fredholm equation of the second kind that can be expanded as a Neumann series (Van Borselen *et al.*, 1996), yielding

$$X_0(\mathbf{x}_B, \mathbf{x}_A; \omega) = \sum_{k=0}^{\infty} (-1)^k \mathcal{K}^k\{X^-(\mathbf{x}_B, \mathbf{x}_A; \omega)\}, \quad (42)$$

where $\mathcal{K}^0\{X^-(\mathbf{x}_B, \mathbf{x}_A; \omega)\} = X^-(\mathbf{x}_B, \mathbf{x}_A; \omega)$, and $\mathcal{K}$ is the following convolutional integral operator:

$$\mathcal{K}\{X^-(\mathbf{x}_B, \mathbf{x}_A; \omega)\} = \int_{\partial\mathbb{D}} X^-(\mathbf{x}_B, \mathbf{x}; \omega)\, X^+_{sc}(\mathbf{x}, \mathbf{x}_A; \omega)\,\mathrm{d}^2\mathbf{x}. \quad (43)$$

In SRME, it is common practice to compute only the first iteration of this scheme (Kelamis and Verschuur 2000), leading to a gather with predicted multiples $X^-_M(\mathbf{x}_B, \mathbf{x}_A; \omega) = \mathcal{K}\{X^-(\mathbf{x}_B, \mathbf{x}_A; \omega)\}$ (where subscript M stands for "multiples") that can be subtracted adaptively from X^- (Verschuur and Berkhout 1997). A similar approach might be applicable to data from shallow receiver arrays, after virtual source redatuming and deconvolution.

CONCLUSION

Virtual source redatuming to a shallow downhole receiver array can be attractive for improving signal quality and repeatability. When this methodology is applied to pressure fields, we retrieve a filtered sum of downgoing and upgoing waves. When applied to vertical particle velocity fields, we retrieve a filtered difference of downgoing and upgoing waves. This observation allows us to decompose downgoing and upgoing wavefields after virtual source redatuming. Knowledge of the medium parameters at the receiver level is not required with this approach since the sensors can be naturally calibrated by an intermediate deconvolution step. After virtual source redatuming and decomposition of the upgoing and downgoing waves, surface-related effects can be removed by a multi-dimensional deconvolution of the upgoing fields with the downgoing fields. Unlike in conventional free-surface demultiple methods, the source wavelet does not need to be estimated as it is effectively removed during deconvolution. We have developed a workflow for virtual source redatuming, wavefield decomposition, and multidimensional deconvolution, which we designed particularly for the recordings by horizontal receiver arrays in the shallow subsurface (20 m–60 m). Because these recordings typically have a high wavenumber content and sparse receiver distributions, we applied preconditioning with a synthetic-aperture-source filter to avoid spatial aliasing.

ACKNOWLEDGMENTS

This research was supported in part by the Dutch Technology Foundation STW, which is the applied science division of NWO, and by the Dutch Technology Program of the Ministry of Economic Affairs. We would like to thank Boris Kashtan of St. Petersburg State University for hosting Joost van der Neut at his institute, and Kees Wapenaar of Delft University of Technology for hosting Dmitry Alexandrov at his institute. These visits have contributed significantly to this paper. The authors would also like to thank Kees Wapenaar for the several useful suggestions that contributed to this paper and to Saudi Aramco for providing the synthetic data.

REFERENCES

Alexandrov D., Bakulin A. and Burnstad R. 2012. Virtual source redatuming of synthetic land data acquired with shallow buried receivers. 74th EAGE Conference and Exhibition, Extended Abstracts, P252.

Amundsen L. 2001. Elimination of free-surface related multiples without need of the source wavelet, *Geophysics* **66**, 327–341.

Amundsen L., Ikelle T. and Berg L.E. 2001. Multidimensional signature deconvolution and free surface multiple elimination of marine multicomponent ocean-bottom seismic data, *Geophysics* **66**, 1594–1604.

Bakulin A.V., Burnstad R.M., Jervis M.A. and Kelamis P.G. 2012. The feasibility of permanent land seismic monitoring with buried geophones and hydrophones. 74th EAGE Conference and Exhibition, Extended Abstracts, X038.

Bakulin A. and Calvert R. 2006. The virtual source method: Theory and case study. *Geophysics* **71**, SI139–SI150.

Bakulin A., Mateeva A., Mehta K., Jorgensen P., Ferrandis J., Sinha Herhold I. et al. 2007. Virtual source applications to imaging and reservoir monitoring, *The Leading Edge* **26**, 732–740.

Barr F.J. 1997. Dual-sensor OBC technology. *The Leading Edge* **16**, 45–51.

Berron C., Forgues E., Jervis M., Bakulin A., and Burnstad R. 2012. Buried sources and receivers in a karsted desert environment. 74th EAGE Conference and Exhibition, Extended Abstracts, X040.

Byun J., Yu J. and Seol S.J. 2010. Crosswell monitoring using virtual sources and horizontal wells, *Geophysics* **75**, 37–43.

Claerbout J.F. 1971. Toward a unified theory of reflector mapping, *Geophysics* **36**, 467–481.

Day A., Klüver T., Söllner W., Tabti H., and Carlson D. 2013. Wavefield-separation methods for dual-sensor towed-streamer data, *Geophysics* **78**, WA55–WA70.

Fan Y., Snieder R., Slob E., Hunziker J., Singer J., Sheiman J. *et al.* 2010. Synthetic aperture controlled source electromagnetics. *Geophysical Research Letters* **37**, L13305.

Fishman L,1991. Exact and approximate solutions of the Helmholtz,Weyl composition equation in scalar wave propagation. *Wave Motion* **14**, 205–224.

Fishman L., McCoy J.J, and Wales S.C. 1987. Factorization and path integration of the Helmholtz equation: Numerical algorithms. *Journal of the Acoustical Society of America*, **81**, 1355–1376.

Fokkema J.T. and Van den Berg P.M. 1993. *Seismic Applications of Acoustic Reciprocity*, Elsevier Science Publishing Co.

Grimbergen J.L.T., Dessing F.J. and Wapenaar K. 1998. Modal expansion of one-way operators in laterally varying media. *Geophysics* **63**, 995–1005.

Grobbe N., Van der Neut J. and Almagro Vidal C. 2013. Flux-normalized elastodynamic wavefield decomposition using only particle velocity recordings. *83rd Annual Meeting, SEG, Expanded Abstracts*.

Haines A.J. and De Hoop M.V. 1996. An invariant imbedding analysis of general wave scattering problems. *Journal of Mathematical Physics* **37**, 3854–3881.

Hanafy S.M. and Schuster G.T. 2007. Target-oriented interferometric tomography for GPR data. *Geophysics* **72**, J1–J6.

Henley D.C. 2012. Interferometric application of static corrections. *Geophysics* **77**, Q1–Q13.

Hunziker J., Slob E., Fan Y., Snieder R. and Wapenaar K. 2012. Two-dimensional controlled source electromagnetic interferometry by multidimensional deconvolution: spatial sampling aspects. *Geophysical Prospecting* **60**, 974–994.

Kelamis P.G. and Verschuur D.J. 2000. Surface-related multiple elimination on land seismic data Strategies via case studies. *Geophysics* **65**, 719–734.

Korneev V. and Bakulin A. 2006. On the fundamentals of the virtual source method. *Geophysics* **71**, A13–A17.

Korneev V., Bakulin A. and Lopez J. 2008. Imaging and monitoring with virtual sources on a synthetic 3D data set from the Middle East. 78th SEG Annual Meeting, Expanded Abstracts, 3204–3208.

Lin T.T.Y. and Herrmann F.J. 2013. Robust estimation of primaries by sparse inversion via one-norm minimization, *Geophysics* **78**, R133–R150.

Majdanski M., Kostov C., Kragh E., Moore I., Thompson M. and Mispel J. 2011. Attenuation of free-surface multiples by up/down deconvolution for marine towed-streamer data, *Geophysics* **76**, V129–V138.

Mehta K., Bakulin A., Sheiman J., Calvert R. and Snieder R. 2007. Improving the virtual source method by wavefield separation. *Geophysics* **72**, V79–V86.

Mehta K., Kiyashchenko D., Jorgensen P., Lopez J., Ferrandis J. and Costello M. 2010. Virtual source method applied to crosswell and horizontal well geometries, *The Leading Edge* **29**, 712–723.

Mehta K., Sheiman J.L., Snieder R. and Calvert R. 2008. Strenghtening the virtual-source method for time-lapse monitoring. *Geophysics* **73**, S73–S80.

Muijs R., Robertsson J.O.A. and Holliger K. 2004. Data-driven adaptive decomposition of multicomponent seabed seismic recordings. *Geophysics* **69**, 1329–1337.

Robertsson J.O.A., Moore I., Vassallo M., Özdemir K., vanManen D.J. and Özbek A. 2008. On the use of multicomponent streamer recordings for reconstruction of pressure wavefields in the crossline direction. *Geophysics* **73**, A45–A49.

Schalkwijk K.M., Wapenaar C.P.A. and Verschuur D.J. 2003. Adaptive decomposition of multicomponent ocean-bottom seismic data into downgoing and upgoing P- and S-waves, *Geophysics* **68**, 1091–1102.

Schuster G.T. and Zhou M. 2006. A theoretical overview of model-based and correlation-based redatuming methods. *Geophysics* **71**, SI103–SI110.

Tatanova M., Mehta K. and Kashtan B. 2011. Virtual refraction tomography: Application to realistic 3D model. 81st SEG Annual Meeting, Expanded Abstracts, 4239–4243.

Van Borselen R.G., Fokkema J.T. and Van Den Berg P.M. 1996. Removal of surface-related wave phenomena-The marine case. *Geophysics* **61**, 202–210.

Van der Neut J. 2013. Downhole interferometric illumination diagnosis and balancing, *Geophysical Prospecting* **61**, 352–367.

Van der Neut J., Bakulin A. and Alexandrov A. 2013. Acoustic wavefield separation using horizontal receiver arrays deployed at multiple depths on land. 83rd Annual SEG Meeting, Expanded Abstracts.

Van der Neut J., Frijlink M. and Van Borselen R. 2012. Data macthing for surface-related multiple attenuation by multidimensional deconvolution. *Geophysical Journal International* **191**, 743–750.

Van der Neut J. and Herrmann F.J. 2013. Interferometric redatuming by sparse inversion. *Geophysical Journal International* **191**, 666–670.

Van Groenestijn G.J.A. and Verschuur D.J. 2009. Estimation of primaries and near-offset reconstruction by sparse inversion: Marine data applications. *Geophysics* **74**, R119–R128.

Verschuur D.J. and Berkhout A.J. 1997. Estimation of multiple scattering by iterative inversion, part II: Practical aspects and examples. *Geophysics* **62**, 1595–1611.

Verschuur D.J., Berkhout A.J. and Wapenaar C.P.A. 1992. Adaptive surface-related multiple elimination. *Geophysics* **57**, 1166–1177.

Wang Y., Grion S. and Bale R. 2010. Up-down deconvolution and subsurface structure: theory, limitations and examples. 80th Annual SEG Meeting, Expanded Abstracts, 1672–1676.

Wapenaar C.P.A. and Grimbergen J.L.T. 1996. Reciprocity theorems for one-way wavefields. *Geophysical Journal International* **127**, 169–177.

Wapenaar K. 1998. Reciprocity properties of one-way propagators. *Geophysics* **63**, 1795–1798.

Wapenaar K. 2006. Green's function retrieval by cross-correlation in case of one-sided illumination. *Geophysical Research Letters* **33**, L19304.

Wapenaar K., Fokkema J. and Snieder R. 2005. Retrieving the Green's function in an open system by cross correlation: A comparison of approaches. *Journal of the Acoustical Society of America* **118**, 2783–2786.

Wapenaar K., Van der Neut J., Ruigrok E., Draganov D., Hunziker J., Slob E. *et al*. 2011. Seismic interferometry by crosscorrelation and by multidimensional deconvolution: A systematic comparison, *Geophysical Journal International* **185**, 1335–1364.

Zhou M., Jian Z., Yu J. and Schuster G.T. 2006. Comparison between interferometric migration and reduced-time migration of common-depth point data, *Geophyscis* **71**, SI189–SI196.